NJC

Accepted Manuscript

This is an *Accepted Manuscript*, which has been through the Royal Society of Chemistry peer review process and has been accepted for publication.

Accepted Manuscripts are published online shortly after acceptance, before technical editing, formatting and proof reading. Using this free service, authors can make their results available to the community, in citable form, before we publish the edited article. We will replace this *Accepted Manuscript* with the edited and formatted *Advance Article* as soon as it is available.

You can find more information about *Accepted Manuscripts* in the Information for Authors.

Please note that technical editing may introduce minor changes to the text and/or graphics, which may alter content. The journal's standard Terms & Conditions and the Ethical guidelines still apply. In no event shall the Royal Society of Chemistry be held responsible for any errors or omissions in this *Accepted Manuscript* or any consequences arising from the use of any information it contains.

ROYAL SOCIETY OF CHEMISTRY

www.rsc.org/njc

Influence of time interval on the phase, microstructure and electrochemical properties of hopeite coating on stainless steel by chemical conversion method

Xian Zhang[a,b,c], Gui-yong Xiao[a,b c], Bing Liu[a,b,c], Cong-cong Jiang[a,b,c], Yu-peng Lu[a,b,c*]

[a] Key Laboratory for Liquid-Solid Structural Evolution and Processing of Materials, Ministry of Education, Shandong University, Ji'nan, 250061, China;

[b] School of Materials Science and Engineering, Shandong University, Ji'nan, 250061, China;

[c] Suzhou Institute, Shandong University, Suzhou, 215123, China

[*]Corresponding author: Tel: 86-0531-88395966; Fax: 86-0531-88395966.

E-mail address: biosdu@sdu.edu.cn (Y. P. Lu)

Abstract

Recently, hopeite coating on metals has attracted more attention due to its potential biomedical application by the zinc phosphate chemical conversion (ZPCC) process. The present study has focused on the time interval necessary for the formation of hopeite coatings by ZPCC method on stainless steel. It was shown that the coatings were composed of hopeite with minor phosphophyllite. Both the coating mass and bath efficiency reached the highest values after ZPCC treatment at 75 ℃ for 30 min. The electrochemical analysis revealed that the coating obtained for 30 min presented the best corrosion resistance. Therefore, the optimum time for the formation of ZPCC coating was 30 min. Adhesion test indicated that the coating was strongly

attached on the substrate.

Keywords: Stainless steel; Hopeite; Zinc phosphate chemical conversion coating; Microstructure; Time interval; Electrochemical corrosion;

1. Introduction

Phosphate chemical conversion (PCC) technology is commonly regarded as the surface pretreatment process of metal, which is widely used as an ideal way to improve surface corrosion resistance, wear resistance, adhesion of the underlying substrate, etc.[1]. This approach plays a significant role in industry, due to its rapid coating formation, the suitability for treatment of irregular surface and the low-cost [1, 2]. The PCC solutions are classified as zinc system, manganese system, iron system, zinc-calcium system, magnesium system and chromate system, which is based on the nature of the metal ion constituting the major component of the PCC solution [1, 3-7]. Among the above systems, ZPCC is used extensively to improve corrosion resistance in industry. ZPCC process is effectively performed on mild steels, galvanized steels, nitrided stainless steel/stainless steel, magnesium alloys, titanium and aluminum. The chemical treatment, electrochemical treatment and hydrothermal treatment are methods reported in the literature which are adapted to fabricate ZPCC coatings [8-17]. Hopeite, as the main phase of ZPCC coating, is commonly used in electric motors, automotive industry and anticorrosive pigments [18]. Furthermore, hopeite, which is the stable phase on the surface of zinc phosphate dental cements, is regarded as the potential versatile biomedical material, due to the high osteogenic property and good biocompatibility[19-21]. In vitro studies have shown that osteogenic and human

fibroblast cells attach and spread well on the hopeite coating which formed on titanium surface [10, 12].

As an important class of steels, stainless steels possess excellent corrosion resistance because of the passive oxide layer on their surface. Furthermore, they have been extensively utilized in our daily life due to the low cost, workability and excellent mechanical performances[22-24]. However, the corrosion behavior of stainless steel has been found in highly aggressive environments and in the body fluid, which leads to the release of harmful ions from stainless steels into the peri-prosthetic environment[25-28]. The severe release will generate harmful effect on human health. For this reason, concerns arise particularly in the surface modification to endow the stainless steels with a protective and biocompatible coating [24, 29, 30]. Untill now, there are numerous methods for surface modification, such as sol-gel [31-34], electrodepositing [9, 35-37], electrochemical [38, 39 40] and plasma nitriding/carburising [41-44].

It is reported that among the common alloying elements, chromium, which exists in the passive oxide layer, impairs the phosphatibility to the largest extent and its content should not exceed 4% [45]. Therefore, it is difficult to develop phosphate coating by traditional chemical conversion method on the surface of stainless steel with the chromium content higher than 4%. Usually, the pretreatment for surface activation or other methods including electroplating, electrophosphating and hydrothermal treatment are adopted to fabricated PCC coatings on stainless steels [1, 9, 14, 38, 46]. Based on previous work [11], the fine and uniform hopeite coating was fabricated on 304 stainless steel (304 SS) and it was also found that the coating

formation was initiated by Fe^{2+} ions. The purpose of this research is to study the influence of the time interval on ZPCC coating, such as phase, microstructure, coating mass, electrochemical properties, etc.

2. Materials and method

2.1 Chemical conversion process

Commercially available 304 SS specimens were used as substrates with the size of 10 × 10 × 1 mm^3. The specimens were abraded using 240-grit emery paper, followed by degreasing in 80 g/L sodium hydroxide solution at 60 ℃ for 15 min. Then, pickling was performed on the specimens in a solution containing 7%V/V of phosphoric acid (85 %) at room temperature for 10 min. Afterwards, activation was performed in a solution of 3 g/L Ti colloids ($Na_4TiO(PO_4)_2$, commercially obtained) at room temperature for 30 s. The samples were then immersed in a bath with the composition of zinc oxide: 25 g/L, phosphoric acid (85 %): 10 ml/L, nitric acid: 30 ml/L, sodium chlorate: 0.2 g/L, calcium nitrate: 5 g/L and citric acid: 5 g/L at 75 ℃ for different duration times from 5 to 45 min with the bath pH value of 2.75.

Before immersion process, the bath solution was cured with 5 g/L pure iron powder (AR, 98 %) at room temperature for 24 hours. The aim of the curing process was to dissolve part of iron powder and increase the concentration of Fe^{2+} in ZPCC bath. After curing, the remained pure iron powder was removed. Finally, the samples were washed with distilled water and dried by blowing air at room temperature.

2.2 Physical and microstructural characterization

For the measurement of coating mass, a digital scale with an accuracy of ± 0.1 mg

was used for the determination of the weight of the samples.

The coating mass (M, g/m^2) was calculated according to Equation (1):

$$M = (m_1 - m_2)/A \quad (1)$$

where m_1 and m_2 are the weights (g) before and after the coatings were stripped, respectively, A is the areas of the substrates (m^2). The stripping was performed in a solution containing 50 g/L of chromium trioxide at 70 ℃ for 10 min. The results of coating mass were the average value of five different measurements and the arithmetic average values were quoted.

For the bath efficiency evaluation, the sludge precipitated during the ZPCC treatment was used to determine the efficiency of the bath [3, 47]. The bath efficiency (E) was calculated according to Equation (2) [3]:

$$E = M/W \quad (2)$$

where E is the bath efficiency, M is the coating mass of the coating, W is the weight of the sludge. The sludge was separated from the ZPCC solution using filter paper from 250 ml ZPCC solution treated 0.05 m^2 substrates and dried at 110 ℃ for 24 h. Then the sludge weight was evaluated using a digital scale with an accuracy of ± 0.1 mg.

The microstructures of the coatings were studied using a SU-70 field emission SEM (FE-SEM). The phase analysis of the coatings were carried out using a Rigaku D/max-γB X-ray diffractometer (XRD), with a scan speed of 4 deg/min between 5 and 80 ° 2θ angle and CuKα radiation, operating at 40 KV and 100 mA.

2.3 Electrochemical evaluation

The corrosion resistance of the samples was evaluated by electrochemical

measurements, which were carried out using a classical three electrodes cell with platinum as counter electrode, saturated calomel electrode (SCE) as the reference electrode, and the uncoated and coated samples with an exposed area of 1 cm^2 as working electrode. The corrosive medium of 0.9 wt. % sodium chloride solution was used. The open circuit potential (OCP), potentiodynamic polarization and electrochemical impedance spectroscopy (EIS) were obtained using a Parstat potentiostat model 2273 at room temperature. The potentiodynamic polarization was measured at constant voltage scan rate of 1 mV/s. The OCP was recorded as a function of time up to 1200 s. The EIS tests were measured at an OCP, with the voltage perturbation amplitude of 5 mV and the frequency range from 100 kHz to 0.01 Hz. The equivalent electrical circuits and electrochemical parameters were obtained by EIS curves, using the ZSimp Win fitting program.

2.4 Contact angle measurements

Contact angle measurements using the sessile drop method were conducted by a water contact angle meter. The water dropped slowly onto the flat samples surface by a microsyringe at room temperature. The images of droplet were photographed after 100 s placed on the surface using a video camera coupled to a light microscope. Then, the contact angle was measured by the imaging software. Three samples were analyzed and two random spots per samples were measured.

2.5 Adhesion test

The tensile strength tests were carried out to obtain the adhesive bond strength of the ZPCC coating to the substrate, according to the modified ASTM C633-01 method

[48]. The schematic diagram of the tensile strength test is given in Fig. 1. Both sides of the coated samples were adhered by modified acrylic adhesive to stainless steel cylinders with 10 mm diameter. The tensile strength tests were carried out at a loading speed of 0.5 mm/min on a RGD-5 electric tension machine at room temperature. The adhesive bond strength was determined from the maximum load recorded. At least ten parallel samples were used and the adhesive strength was the average of five steady results among the ten samples. The standard deviation was also quoted.

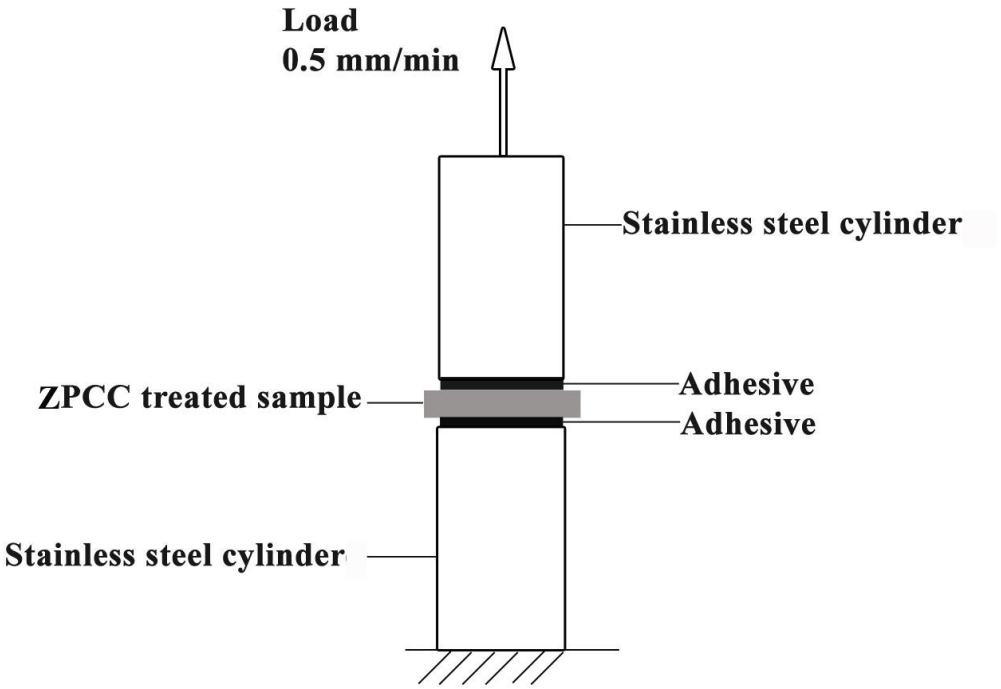

Fig. 1 The schematic diagram of the tensile strength test for adhesion test.

3. Results and discussion

3.1 Coating mass

The relationship between the time internal and coating mass of ZPCC coatings as well as sludge weight of the solutions obtained at 75 ℃ is shown in Fig. 2. It is

clearly observed that both the coating mass and sludge weight rise with the increase of reaction time. As time increases from 5 to 45 min, the coating mass changes from 7.589 ± 0.73 to 13.991 ± 0.68 g/m^2, while the sludge weight increases from 0.096 to 0.146 g. Nevertheless, the two curves show a non-linear pattern. Herein, both of them vary significantly between 30 and 45 min. The coating mass increases slowly from 13.452 ± 0.60 to 13.991 ± 0.68 g/m^2. On the contrary, the sludge weight increases sharply from 0.1099 to 0.1461 g.

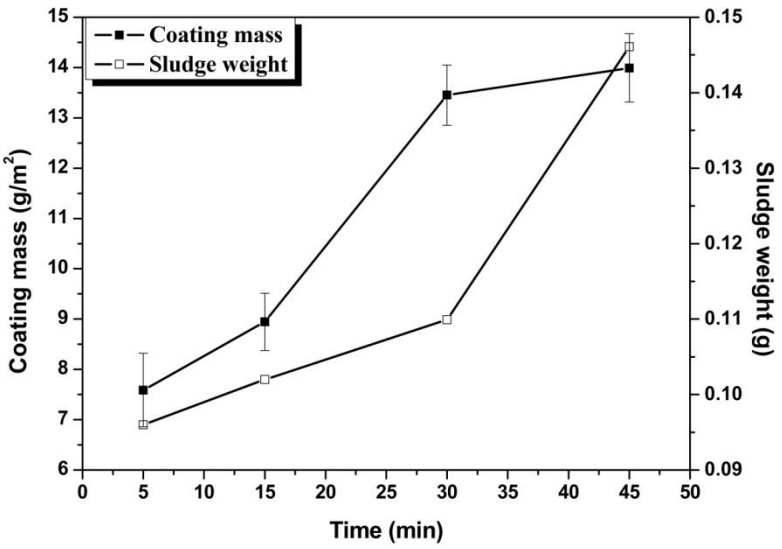

Fig. 2 The coating mass and sludge weight of the ZPCC coating vs. time curves at 75℃.

At the initial stage of conversion process, the remaining passivation layer is dissolved firstly and the nucleation rate is relatively low. Therefore, the increase of coating mass from 5 to 15 min is slow. Subsequently, the crystal growth, reorganization and the secondary crystallization contribute to the improvement of

coating mass [1], which results in the rapid increase of coating mass from 15 to 30 min. The saturation point of coating formation and the dissolution of the crystals result in the no difference of the coating mass between 30 and 45 min [1, 49]. The sludge weight also enhances with the increase of duration time. The excessive sludge formation may inhibit the formation of coating and even result in low corrosion resistance [1].

The coating mass is a method of quality control in industry, which is related to the thickness and homogeneity of the coating [1, 11]. Therefore, in this study, the bath efficiency is calculated by coating mass rather than thickness, due to the uneven nature of the substrate and the coating [1, 3]. As shown in Fig. 3, by increasing the time from 5 min to 30 min the bath efficiency gradually increases from 3.95 to 6.12%, and the value of that decreases to 4.97% after 45 min treatment. The coating mass has a slight difference between 30 and 45 min due to the decrease of bath efficiency. It is seen that the maximum value of bath efficiency is obtained after 30 min of treatment. Accordingly, the coating obtained at 75 ℃ for 30 min is more uniform and thus possesses better properties.

The XRD pattern of the sludge is listed in Fig. 4. It is indicated that the sludge is mainly consisted of amorphous compounds. The crystalline compounds are hardly to determine their composition due to the amorphous background. It is obvious that the sludge consists of some other insoluble tertiary phosphate salt, e.g. $Zn_3(PO_4)_2$ and $Fe_3(PO_4)_2$ [1], rather than hopeite. The formation of sludge has an adverse influence on the formation of hopeite, which would decrease the bath efficiency (Fig. 3). Moreover, the sludge is considered as the hazardous waste materials and should be subject to

strict regulations as to disposal. The efforts of current researches are focused on recovering and reusing various sludge components [1, 47].

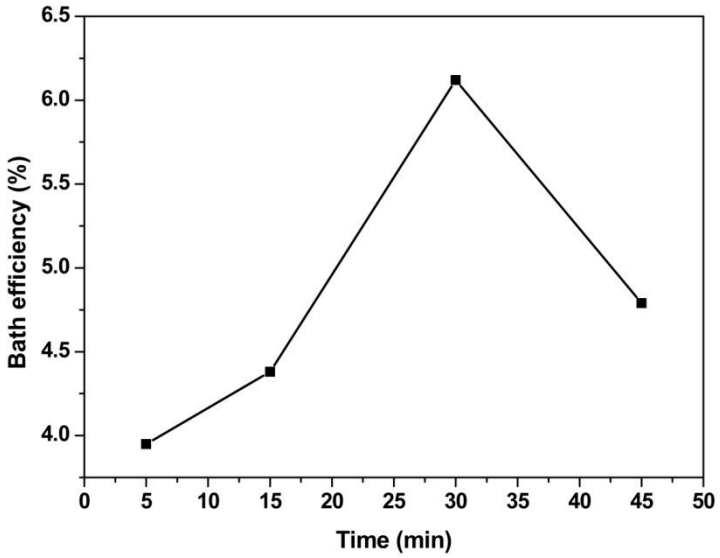

Fig. 3 The relationship between bath efficiency and time for 304 SS samples ZPCC treated at 75 ℃ with bath pH of 2.75.

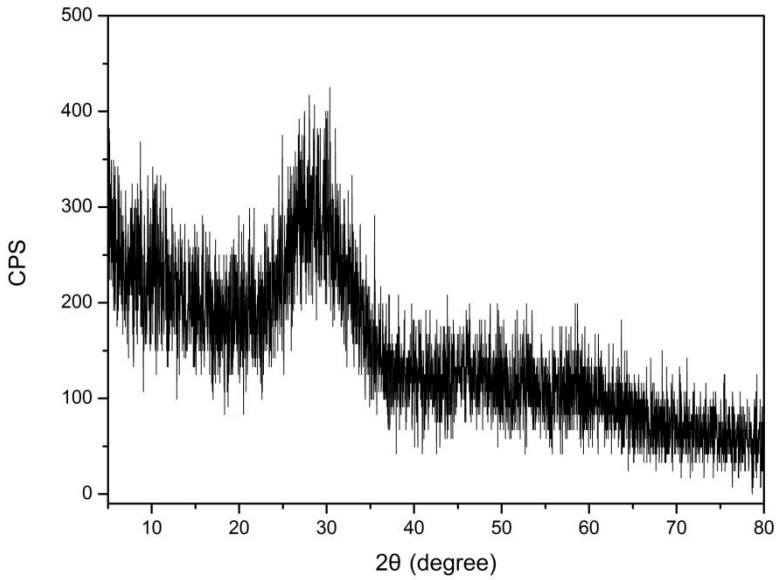

Fig. 4 XRD pattern of the sludge, precipitated from ZPCC solution.

3.2 Phase analysis

Fig. 5 shows the XRD patterns of ZPCC coatings treated at 75 ℃ for different treatment time. It can be seen that the coatings consist of hopeite (JCPDS # 37-0456) and minor phosphophyllite (JCPDS # 29-1427). The ZPCC coating is formed on the substrate according to the reactions as follows:

$$3\,Zn^{2+} + 2\,H_2PO_4^- + 4H_2O \rightarrow Zn_3(PO_4)_2 \cdot 4H_2O \downarrow + 4H^+ \quad (3)$$

$$Fe^{2+} + 2Zn^{2+} + 2H_2PO_4^- + 4H_2O \rightarrow Zn_2Fe(PO_4)_2 \cdot 4H_2O \downarrow + 4H^+ \quad (4)$$

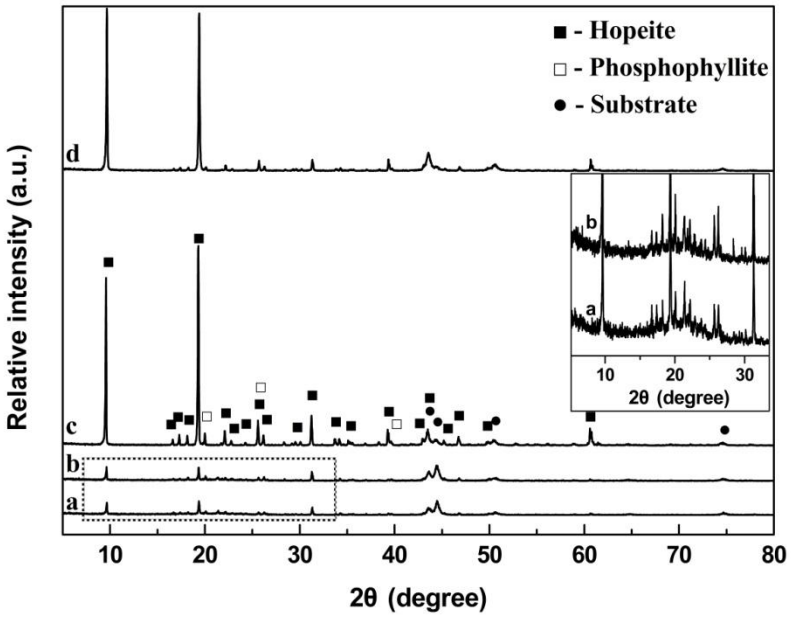

Fig. 5 XRD patterns of the samples ZPCC treated for different times at 75℃. (a) 5 min, (b) 15 min, (c) 30 min, (d) 45 min. The inserted image shows local high magnification of the black rectangle.

All of the coatings formed with different times have similar phase spectra, although with various relative peak intensities. The narrow and intense peaks indicate a high crystallinity. As shown in Fig. 5, the relative intensities of peaks enhance with

the increase of duration time, indicating continuous formation of the coating. As shown in Fig. 6, the diffraction intensity variations of the (020), (040) and (241) plane of coatings, the peaks of which are at 9.7°, 19.4° and 31.3°, increase with duration time prolongation. During the ZPCC treated from 5 to 30 min, all the intensities of (020), (040) and (241) plane increase and reach the max values after 30 min of treatment, which may influence the properties of the coating. Among the planes, the diffraction intensity of the peak along the (040) plane obviously increases to the maximum after ZPCC treated for 30 min (Fig. 5c), which implies the preferred epitaxial growth of hopeite along the plane. However, the intensities of peaks are lower for the sample after 45 min treatment than those of 30 min. This might be attributed to the crystal refinement as well as the redissolution and reorganization of the crystal as mentioned in section 3.1 [50].

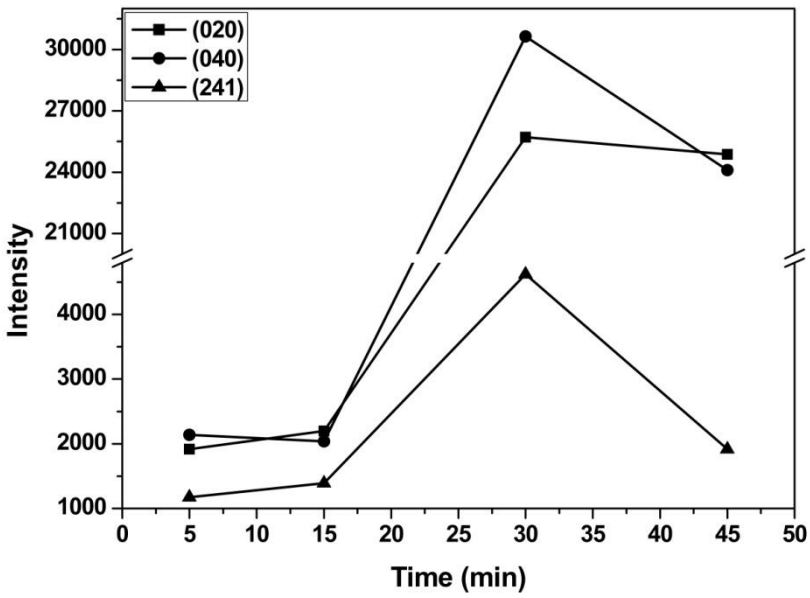

Fig. 6 The planes variation of the hopeite coating with different times according to XRD spectra.

Additionally, it is clear that amorphous humps are found at 2θ of 15-25° in XRD patterns of samples (the inserted images in Fig. 5 a-b), and they disappear with the duration time increase (Fig. 5 c-d), which suggests the existence of the amorphous phase during the coating formation. The formation of amorphous is one of the stages among the ZPCC coating formed, afterward, the next stage is crystallization and growth of the coating [1].

As reported, hopeite, as a potential versatile biomedical material, is biocompatible and its powder could be transformed into hydroxyapatite (HA) in alkaline medium containing saturated with Ca^{2+} [20, 21]. In view of this, more efforts have been focused on preparing the hopeite coating using chemical conversion methods [11, 12]. Compared with hopeite, phopsphophyllite, which is formed at the surface of contact with the substrate, has better corrosion resistance in sodium chloride solution or other aqueous media because of its chemical stability [1, 51].

3.3 Microstructural characterization

The FE-SEM images of the coatings obtained at 75 ℃ for different duration times are shown in Fig. 7. It can be seen that a continuous coating fully covered the substrate. The morphology of the crystals changes from plate-like to slabby-like, with the size of 4-15 μm. The crystal size of coating treated for 5 min is 8-10μm, while that treated for 15 min is 4-8 μm. It reveals that the coating shows the finer crystal size for a longer duration time (Fig. 7a-b), which indicates the formation of new crystal [51]. The growth of crystal and the secondary crystallization contribute to the increase of coating mass for the duration times from 15 to 30 min (Fig. 7b-c) [1]. The crystal of

coating formed for 45 min treatment has a size of about 5-8 μm, which is smaller than that for 30 min treatment, with a crystal size of about 5-15 μm (Fig. 7c-d). This could explain the lower peak intensities of XRD pattern of coating formed for 45 min than those for 30 min.

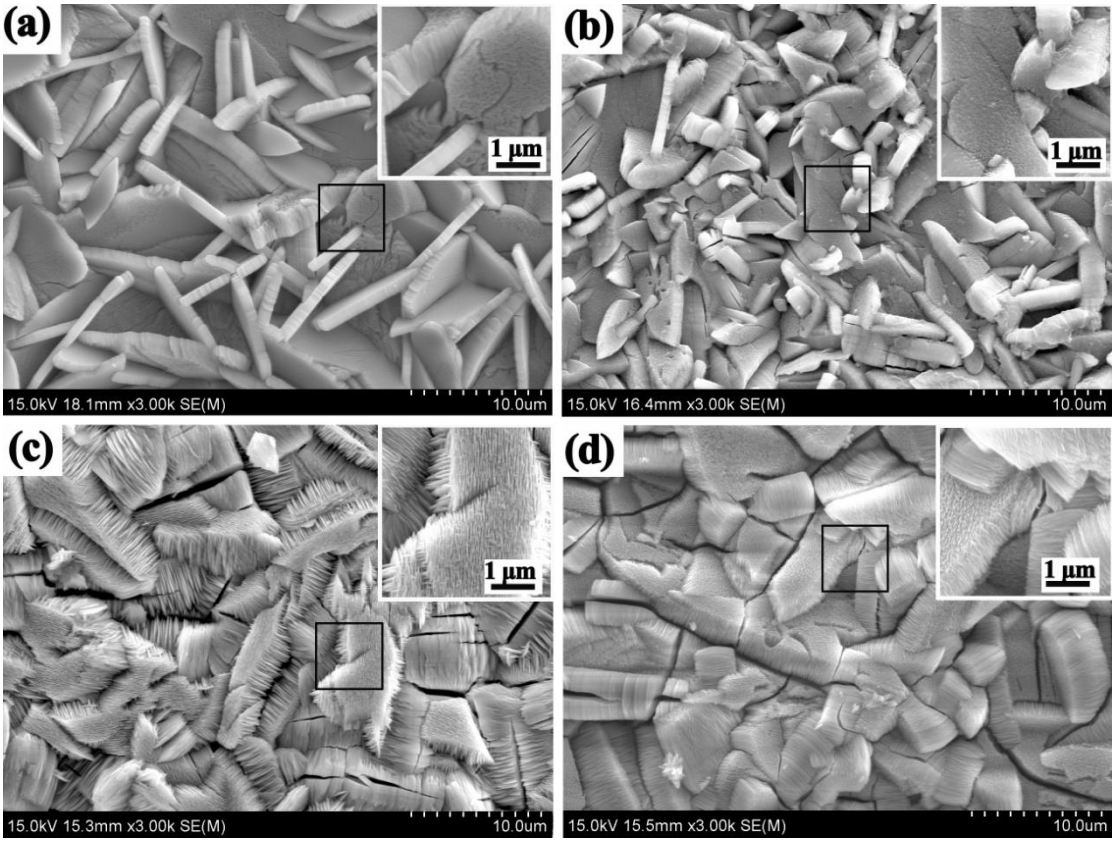

Fig. 7 FE-SEM images of the coatings ZPCC treated for different times at 75℃. (a) 5 min, (b) 15 min, (c) 30 min, (d) 45 min. The inserted images are high magnification images of the black rectangle.

At the same time, the microscopic features of crystal surface also change with time, the surface and slab edges of crystals become rough (Fig. 7 and 8) due to the dissolution of crystals in ZPCC solution for a long time. According to equations 3 and

4, the concentration of H^+ ions increases during the formation of coatings, which causes the dissolution of crystals [20]. Therefore, the surfaces and edges of the crystals become rougher (Fig. 8). Distinct nanoscale structures are also found (Fig. 8). The nanoscale structures may enhance the adhesion and proliferation of the cells, which may have potential significance to biomedical application [52, 53]. Recently, hopeite has been considered a potential versatile biomedical material [20]. The cells attach and spread well on hopeite surface by cell culture study using human fibroblast and osteogenic cells [12, 54].

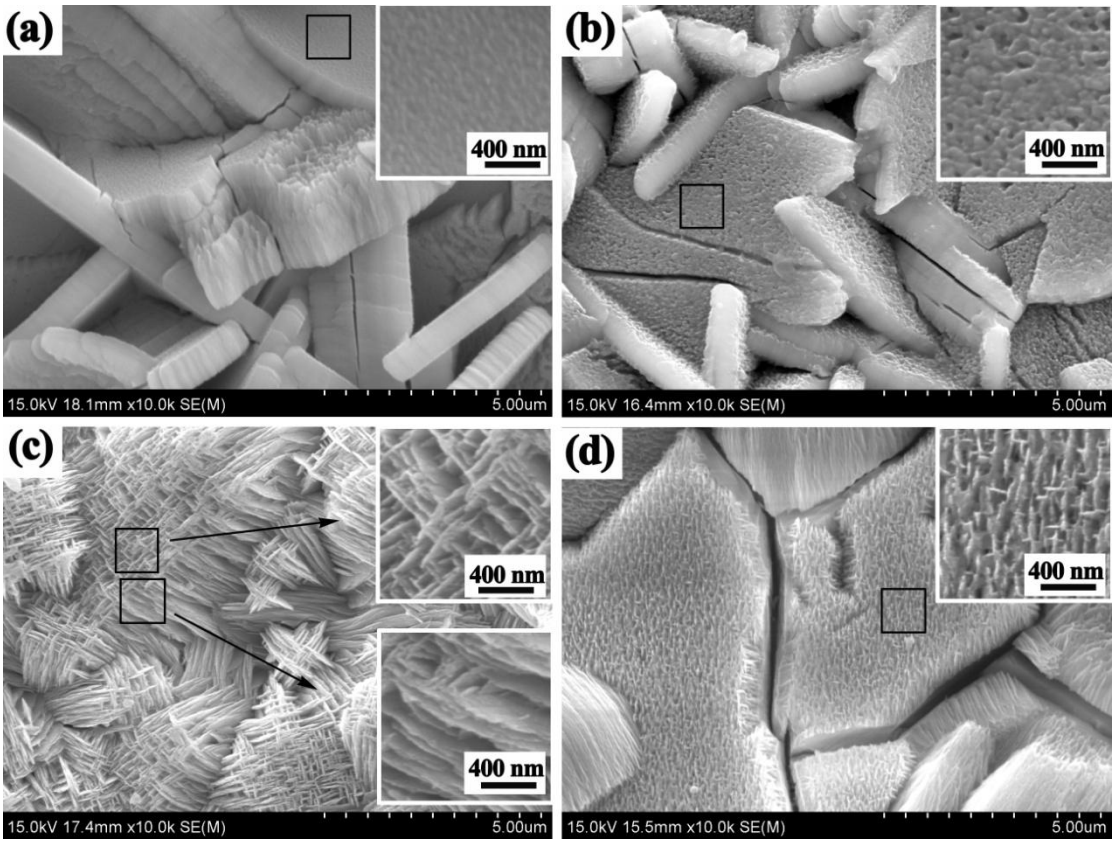

Fig. 8 FE-SEM images of crystal surfaces of the hopeite coatings for different times at 75℃. (a) 5 min, (b) 15 min, (c) 30 min, (d) 45 min. The inserted images are high magnification images of the black rectangle.

The formation of ZPCC coating is defined into four stages: the dissolution of the substrate, amorphous formation, crystallization and growth of the crystals, finally crystal reorganization [1, 11, 51]. The dissolution of the substrate, generating the Fe^{2+}, is considered to be a prerequisite stage for the start of ZPCC process [1]. Furthermore, it is the key factor of the diffusion of Fe^{2+} in the initiate formation of the coating. However, it is difficult to obtain the enough Fe^{2+} ions from the stainless steel surface, due to the presence of passive oxide coating. In this study, Fe^{2+} ions are compensated by the curing process to accelerate the formation of coating. The abundance of Fe^{2+} ions in the interface of the substrate/solution leads to the precipitation of phosphophyllite at the beginning of ZPCC process in amorphous state, which is found in Fig. 5 a-b. Then, the nuclei of hopeite start and involve crystallization and growth, which increase rapidly with time. The reprecipitation and crystal crystallization is the last stage (Fig. 7). At the last stage, the microscopic features of crystal surface changes obviously and the nanoscale structures are generated.

3.4 Electrochemical investigation

The changes of OCP as a function of time for the ZPCC coated samples in 0.9 wt. % sodium chloride solution are given in Fig. 9. The value of OCP does not show any sharp change for different times. For the coated samples after 5 and 15 min treatment, the OCP values take a longer time to attain the steady potentials. The OCP of the ZPCC coatings for 30 min rapidly changes during the first 200 s, then asymptotically tend towards the steady potential around -0.25 V, whereas that for 45 min remains constant potential after 500 s. This could be due to the uniform and fine

coating on the substrate.

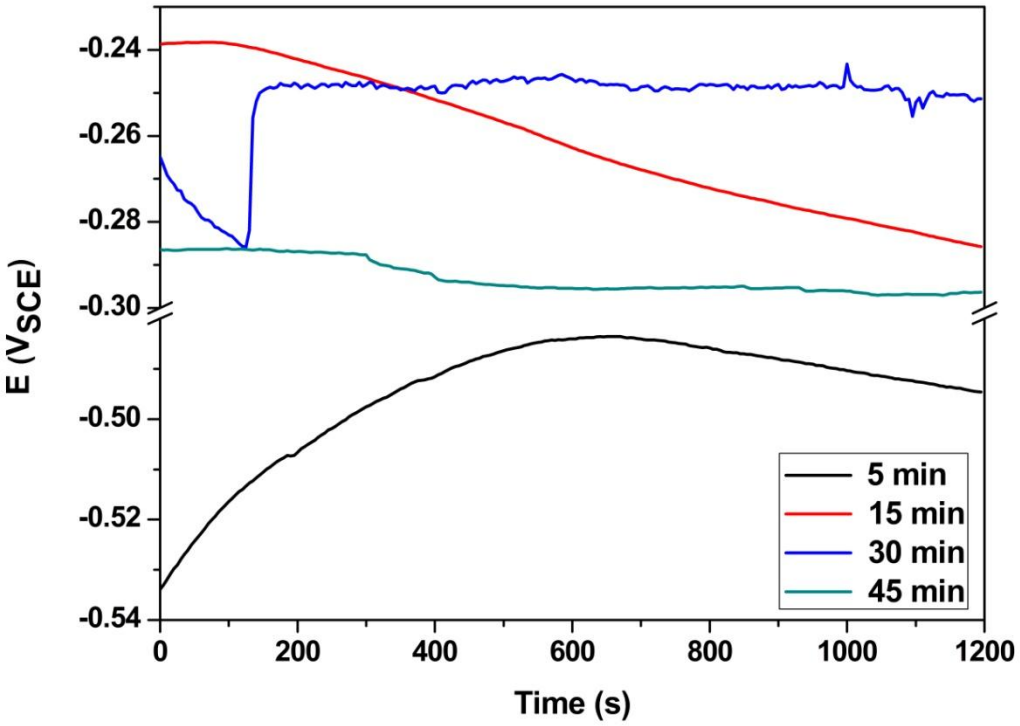

Fig. 9 Variation of the open circuit potential as a function of time in a 0.9 wt. % sodium chloride solution for samples ZPCC treated for different times at 75℃.

Potentiodynamic polarization curves for the ZPCC coatings treated at 75 ℃ for different times and the uncoated sample of 304 SS in a 0.9 wt. % sodium chloride solution are presented in Fig. 10. The electrochemical parameters used to evaluate the properties of the coating are as follows by potentiodynamic polarization curves. The polarization resistance (R_p), which represents the corrosion properties of samples, was calculated using Equation (5) [11, 55]:

$$R_p = \beta_a \cdot \beta_c / (2.303\, I_{corr}\ (\beta_a + \beta_c)) \quad (5)$$

where R_p is the polarization resistance, I_{corr} is the corrosion current density, β_a is

anodic Tafel slope and β_c is cathode Tafel slope. The porosity percentage of ZPCC coating was calculated according to Equation (6) [56, 57]:

$$P = \left(R_{p,s}/R_p\right) \times 10^{-\left(\Delta E_{corr}/\beta_a\right)} \times 100\% \quad (6)$$

where P is the total coating porosity percentage, R_{ps} is the polarization resistance of uncoated sample, R_p is the polarization resistance of coated substrate, ΔE_{corr} is the difference between corrosion potentials of coated and uncoated sample, β_a is anodic Tafel slope of the uncoated sample. Finally, the corrosion protection efficiency was calculated using Equation (7) [3, 16]:

$$P_e\% = (1 - I_{corr}/I_{corr}^0) \times 100 \quad (7)$$

where P_e is the corrosion protection efficiency of the coating, I_{corr} and I_{corr}^0 are the corrosion current density of the coated and uncoated samples, respectively.

Table 1 summarizes the electrochemical parameters, such as corrosion potential (E_{corr}), corrosion current density (I_{corr}), polarization resistance (R_p), the porosity percentage (P) and the corrosion protection efficiency (P_e), of the coated and uncoated samples, which are calculated from Fig. 10 using the Tafel extrapolation method. Fig. 11 shows the schematic diagram of the Tafel extrapolation method.

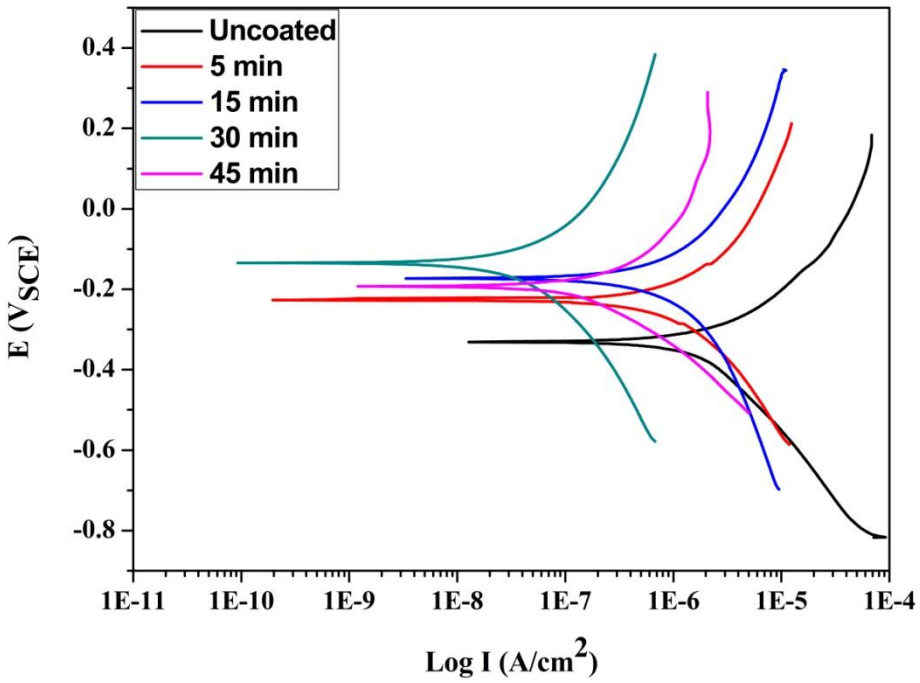

Fig. 10 Potentiodynamic polarization curves of samples for different times at 75℃ and uncoated sample in 0.9 wt. % sodium chloride solution.

Table 1 The results of potentiodynamic corrosion tests in 0.9 wt. % sodium chloride solutions.

	E_{corr} (V_{SCE})	I_{corr} (μA/cm^2)	R_p, ×10^3 (Ω·cm^2)	P (%)	P_e (%)
Uncoated	-0.33	1.98	3.06	--	--
5 min	-0.23	0.884	11.4	8.63	55.35
15 min	-0.172	0.789	18.8	2.71	60.15
30 min	-0.131	0.035	623	0.0514	98.2
45 min	-0.164	0.127	216	0.32	93.6

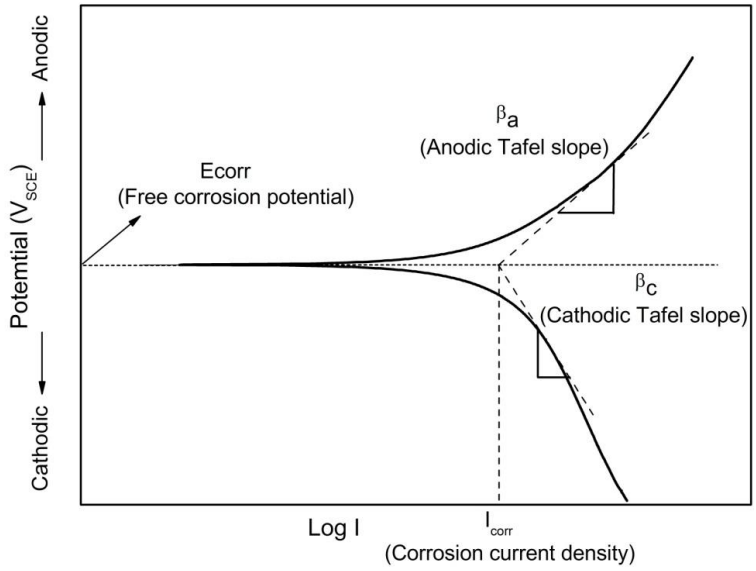

Fig. 11 Schematic illustration of the Tafel extrapolation method.

It is noted that the E_{corr} obtained from the polarization curve is lower than that is determined from the OCP, which is due to the scan rate effect on the Tafel slopes and the disturbance of the charging current [58]. It is clear that the polarization curve assigned for samples with coatings shows a decrease of I_{corr}, the increase of E_{corr} and R_p distinct as compared with those of 304 SS uncoated sample, indicating that the ZPCC coating possesses better corrosion resistance than uncoated sample in a 0.9 wt. % sodium chloride solution. The better corrosion protection is provided by ZPCC coatings due to the chemical stability of phosphophyllite [50]. On the other hand, all the coatings show similar morphology of the crystals and comparison among the curves of samples treated for different times reveal that I_{corr} decreases as well as E_{corr} increases with increase of duration time. These results indicate that the corrosion resistance of the ZPCC coatings is improved by increasing the time up to 30 min, and

this is in accordance with the change of microstructure displayed in Fig. 7 that the crystal assembles tightly and the coating mass increases to higher value (Fig. 2).

It can be seen in Fig. 12 that by increasing the duration time from 5 to 45 min, the corrosion protection efficiency and the polarization resistance increase, while the porosity percentage decreases continuously. However, with the increase of treatment time from 30 to 45 min, both the corrosion protection efficiency and the polarization resistance decrease, while the porosity percentage increases. That is to say, the ZPCC coating treated at 75 ℃ for 30 min shows the greatest corrosion resistance. As mentioned before, by increase the duration time the coating changes obviously with finer, denser crystals as well as higher coating mass which can act as superior corrosion protection.

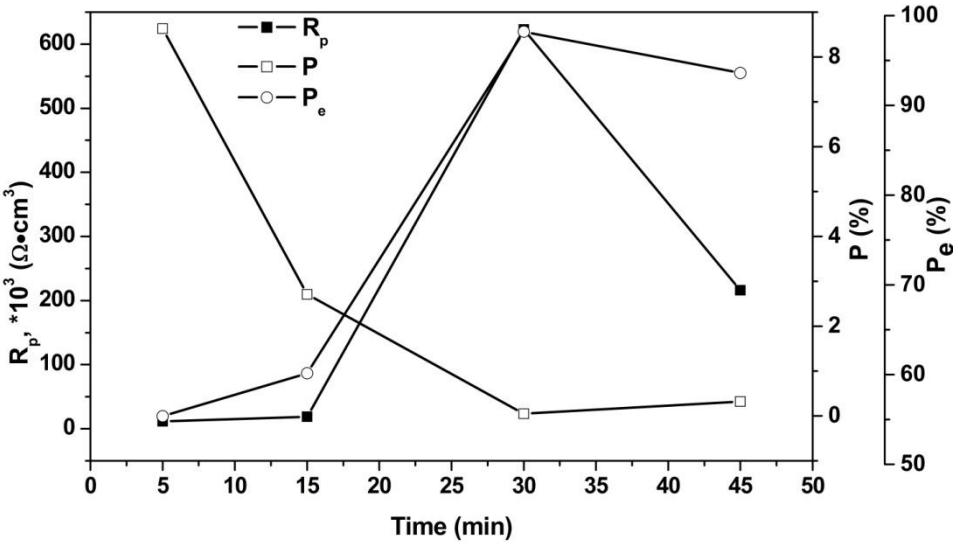

Fig. 12 The variation of the corrosion protection efficiency, the polarization resistance and the porosity percentage as a function of time obtained from potentiodynamic polarization curves.

The EIS measurement is an important and effective tool to determine the electrochemical corrosion behavior of the coating, as well as gives the information about the microstructure of the coating [12, 13, 59]. The EIS characteristics of coated and uncoated samples in a 0.9 wt. % sodium chloride solution conducted at OCP are shown in Fig. 13, as Nyquist (Fig. 13a), Bode impedance (Fig. 13b) and Bode phase angle plots (Fig. 13c), respectively. The insert picture is the enlarged plot of the uncoated sample for better visualization due to the small dimension of Nyquist plots for the uncoated sample and the coated sample treated for 5 min. It can be seen that the shapes of Nyquist plot of coated and uncoated samples are very different, which implies that the corrosion process of them may have different mechanisms (Fig. 13a). Furthermore, the Nyquist plot indicates that the coated samples possess high polarization resistance and impart better protective characteristics than the uncoated sample.

Fig.13b showing the |Z| Bode plot exhibits an increase in impedance value with the increase of duration time. The increase in the impedance value observes for coating after 30 min indicated an enhancement in corrosion resistance of the coating. The Bode plot for the ZPCC coatings carried out after 30 min treatment displays a maximum total impedance (|Z|) value, which is found to be higher than those measured for the other specimens. This phenomenon is indicative of the fact that the coating obtained for 30 min has a high resistivity in physiological saline solution. The Bode plot in phase angle of all samples show the same tends, the phase angle shows the large shift toward to -90° at high frequencies and an inverse shift is observed at

low frequencies. It is reported that the phase angle at high frequency is a response for the pores or even the degradation of the coating, while that at low frequency is a good criterion for the attack of the exposed substrate [60].The samples after ZPCC treated show high phase angles due to the formation of hopeite coatings. The highest phase angle of the sample obtained for the treatment time of 30 min at high frequency region is attributed to the higher coating mass (Fig. 2) and the lowest porosity percentage (Table 1). The result is in good agreement with the results of the OCP and the polarization curves.

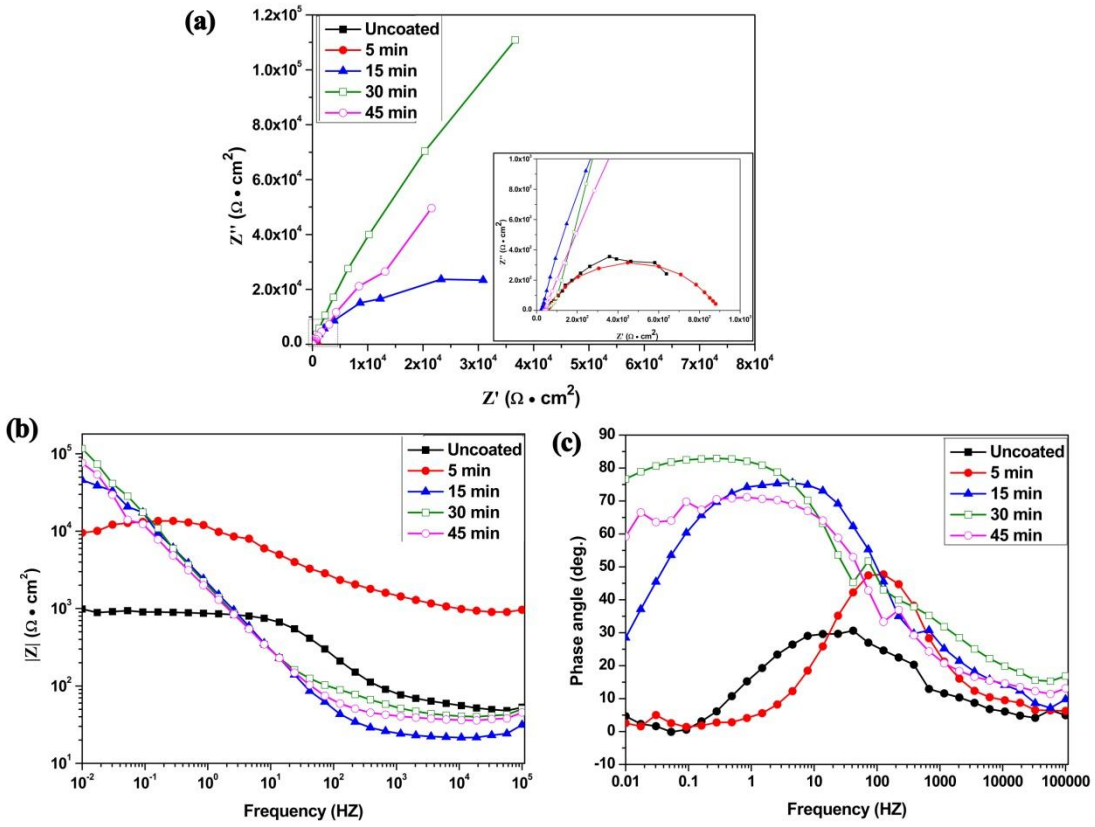

Fig. 13 Impedance spectra presented in a Nyquist plot (a), Bode phase angle (b), and Bode amplitude plots (c) for coated samples with ZPCC treatment for different times and uncoated sample in 0.9 wt. % sodium chloride solution.

The equivalent electrical circuit used to simulate the EIS results is shown in Fig. 14, which is based on the typical model used by many researchers [7, 8, 12, 13, 61, 62]. A good correspondence between the measured and fitted samples is obtained, using the ZSimp Win fitting program. In the electrical circuit, R_s, R_c, R_{ct}, C_c and C_{dl} are the solution resistance, coating resistance, transfer resistance, coating capacitance and double layer capacitance, respectively.

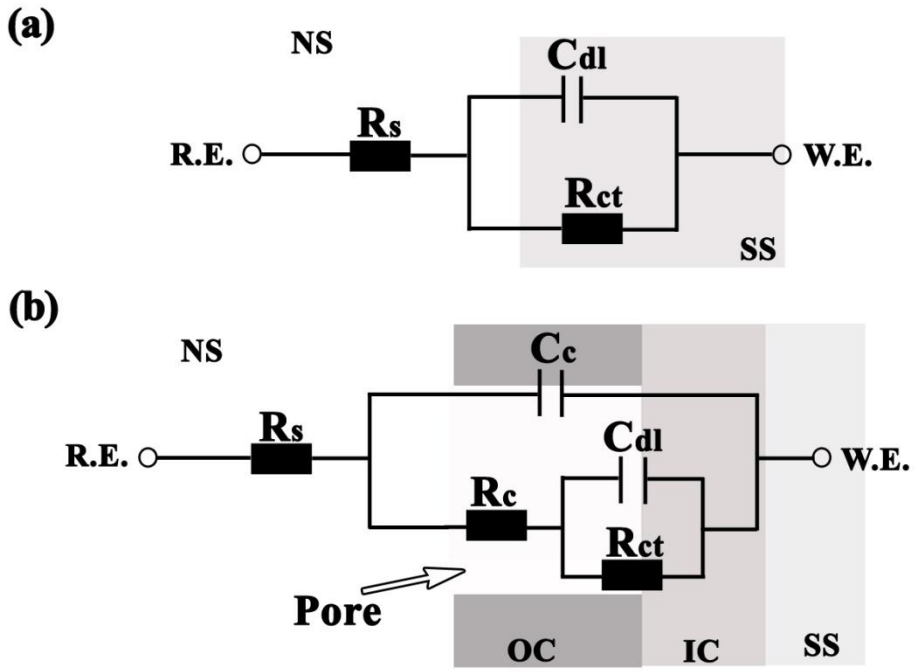

Fig. 14 Equivalent electrical circuits used to model the impedance behavior of uncoated sample (a) and coated samples (b). NS: Normal saline, SS: Stainless steel, OC: Outer coating, IC: Inner coating, R.E.: Reference electrode, W.E.: Working electrode.

Thus, the ZPCC coating impart better corrosion resistance for the substrate, due to the chemical stability of the phosphophyllite and the insoluble hopeite. Among the samples treated for different times, the one treated for 30 min shows the best protection for the substrate. Under this condition, the coating has the lowest I_{corr} and P, the highest E_{corr}, R_p and P_e.

Fig. 15 shows the FE-SEM images of cross-sectional of coating formed at 75 ℃ for 30 min. It is shown that the ZPCC coating consists of two layer, one is the outer coating and another is inner coating [13]. The outer coating is a loose one, while the inner is more compact. The outer coating is porous layer which results from the dissolution of the crystal. This result is in agreement with the EIS result and the mechanism of the ZPCC coating formation.

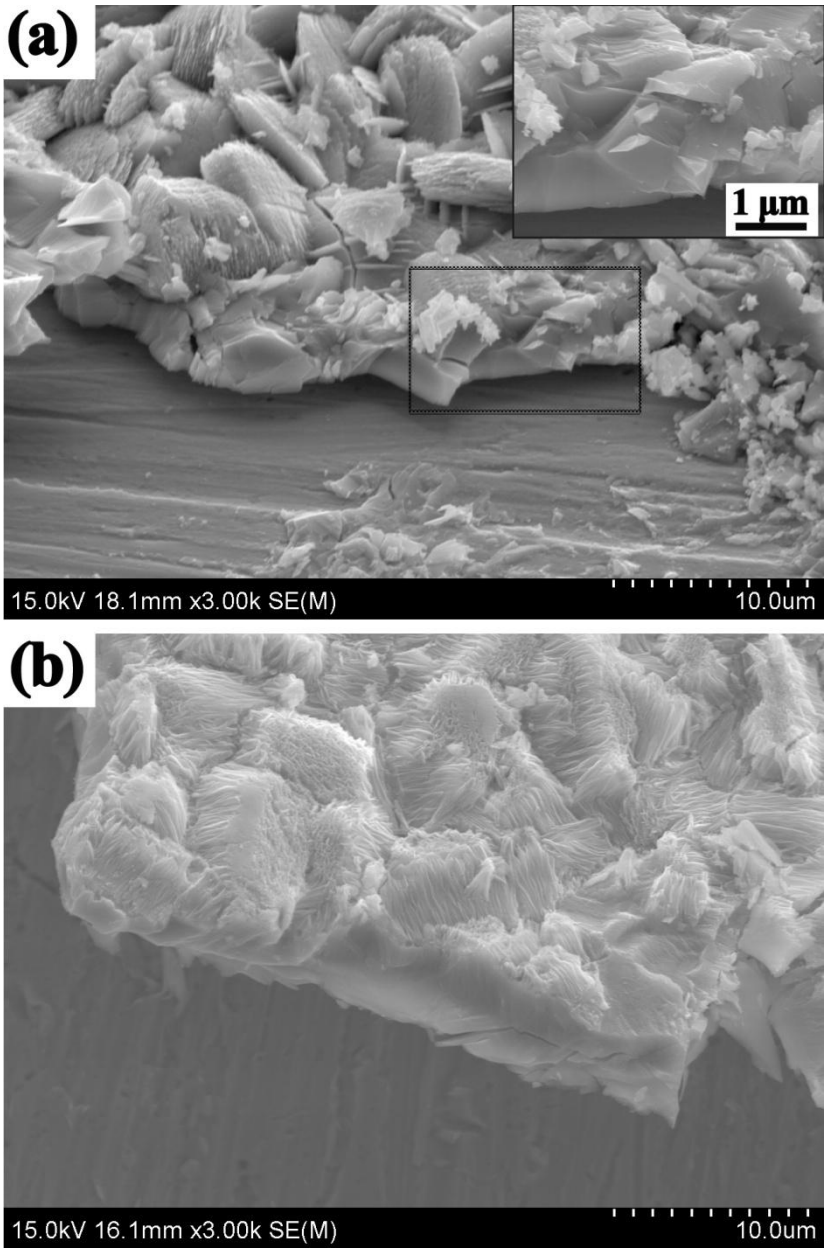

Fig. 15 FE-SEM images of the cross-sectional of coating formed after 30 min treatment. The inserted image is high magnification images of the black rectangle.

3.5 Contact angle measurements

The contact angles measured on 304 SS uncoated sample and the coated sample, treated at 75 ℃ for 30 min, are 95.99 ± 2.88 and 25.38 ± 2.25 °, respectively. The shapes of water dropped on the surface of uncoated and coated samples are

demonstrated in Fig. 16. The result shows that the coated sample is more hydrophilic than substrate surface, which is due to the variation of chemical composition and the difference in surface roughness. The hydrophilic surface of coating is determined by the chemical composition and surface microstructure [63, 64]. The dominant phase of the coating is hopeite, which performs a good hydrophilicity [65]. The roughness of coating is increased by nanoscale structure on the crystal (Fig. 8c), while the value of contact angle decreases with the increase of roughness [66]. The hydrophilic surface of the coating may enhance the cell adhesion of biomaterials [67].

3.6 Adhesion test

According to the result of adhesion test, the determined tensile strength of coated samples, which are treated at 75 ℃ with bath pH of 2.75 for 30 min, between the ZPCC coating and the substrate is 16.38 ± 2.2 MPa. As a comparison, the value is a little higher than that of zinclipscombite coating on 316 stainless steel surface by hydrothermal treatment [9]. The ZPCC coatings have been known as contiguous and porous, which could lead to the highly adherent between the organic coating and the substrate [1].

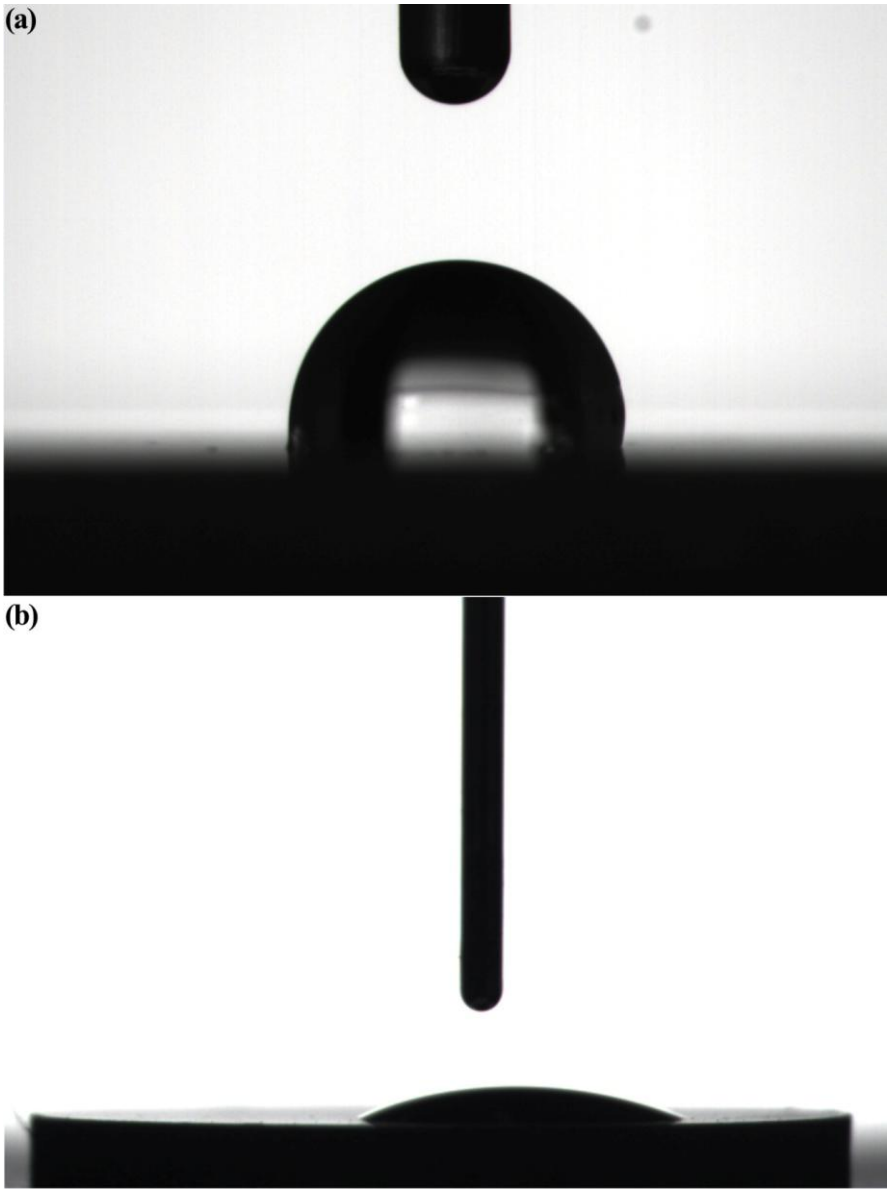

Fig. 16 Shape of water droplets on the coating surface treated at 75℃ for 30 min and uncoated sample.

4. Conclusion

By fabricating a hopeite coating on 304 SS, the effects of time interval on coating mass, bath efficiency, phase, microstructure and electrochemical corrosion of the coatings were investigated. It was shown that the coating formed for different duration times have similar phase composition and crystal shape. The coating mass, bath efficiency and corrosion resistance of coatings increased with the increase of

duration time. The coating after 30 min treatment had the highest bath efficiency and the best corrosion resistance. Therefore, the treatment of 30 min can be considered as the optimum time for the formation of ZPCC coating. The coating treated for 30 min showed a hydrophilic surface, and its tensile strength was 16.38 ± 2.2 MPa. The uniform ZPCC coating may have potential biomedical use due to the better corrosion resistance and the higher adhesive strength. Further studies such as biocompatibility are being undertaken.

Acknowledgements

This work was supported by Jiangsu Province Science Foundation for Youths (BK20140412), Shandong Province Young and Middle-aged Scientists Research Awards Fund (BS2013CL030), Shandong Provincial Science and Technology Development Plan (2014GGX102031) and Independent Innovation Foundation of Shandong University of China (2015JC018).

References

1. T. S. Narayanan, *Rev. Adv. Mater. Sci*, 2005, 9, 130-177.
2. R.-C. Zeng, F. Zhang, Z.-D. Lan, H.-Z. Cui and E.-H. Han, *Corros. Sci.*, 2014, 88, 452-459.
3. M. Fouladi and A. Amadeh, *Electrochim. Acta*, 2013, 106, 1-12.
4. G. Li, J. Lian, L. Niu and Z. Jiang, *Adv. Eng. Mater.*, 2006, 8, 123-127.
5. M. Morks, *Mater. Lett.*, 2004, 58, 3316-3319.
6. C.-M. Wang, H.-C. Liau and W.-T. Tsai, *Surf. Coat. Tech.*, 2006, 201, 2994-3001.

7. P. Campestrini, E. Van Westing and J. De Wit, *Electrochim. Acta*, 2001, 46, 2631-2647.

8. K. Abdalla, A. Rahmat and A. Azizan, *J. Coat. Technol. Res.*, 2013, 10, 133-139.

9. A. Valanezhad, K. Tsuru, M. Maruta, G. Kawachi, S. Matsuya and K. Ishikawa, *Surf. Coat. Tech.*, 2010, 205, 2538-2541.

10. A. Valanezhad, K. Tsuru, M. Maruta, G. Kawachi, S. Matsuya and K. Ishikawa, *Surface and Coatings Technology*, 2012, 206, 2207-2212.

11. X. Zhang, G.-Y. Xiao, Y. Jiao, X.-C. Zhao and Y.-P. Lu, *Surf. Coat. Tech.*, 2013.

12. X.-C. Zhao, G.-Y. Xiao, X. Zhang, H.-Y. Wang and Y.-P. Lu, *J. Phys. Chem. C.*, 2014.

13. Q. Li, S. Xu, J. Hu, S. Zhang, X. Zhong and X. Yang, *Electrochim. Acta*, 2010, 55, 887-894.

14. J. Flis, J. Mańkowski, T. Zakroczymski and T. Bell, *Corros. Sci.*, 2001, 43, 1711-1725.

15. S. Jegannathan, T. Sankara Narayanan, K. Ravichandran and S. Rajeswari, *Electrochim. Acta*, 2005, 51, 247-256.

16. B.-L. Lin, J.-T. Lu and G. Kong, *Corros. Sci.*, 2008, 50, 962-967.

17. D. Susac, X. Sun, R. Li, K. Wong, P. Wong, K. Mitchell and R. Champaneria, *Appl. Surf. Sci.*, 2004, 239, 45-59.

18. P. Parhi, V. Manivannan, S. Kohli and P. McCurdy, *Mater. Res. Bull.*, 2008, 43,

1836-1841.

19. L. Herschke, I. Lieberwirth and G. Wegner, *J. Mater. Sci. Mater. M.*, 2006, 17, 95-104.

20. L. Herschke, J. Rottstegge, I. Lieberwirth and G. Wegner, *J. Mater. Sci. Mater. M.*, 2006, 17, 81-94.

21. S. Shibli and A. Jayalekshmi, *Appl. Surf. Sci.*, 2008, 254, 4103-4110.

22. K. Lo, C. Shek and J. Lai, *Mat. Sci. Eng. R*, 2009, 65, 39-104.

23. D. Addari, B. Elsener and A. Rossi, *Electrochim. Acta*, 2008, 53, 8078-8086.

24. E. Faure, P. Lecomte, S. Lenoir, C. Vreuls, C. Van De Weerdt, C. Archambeau, J. Martial, C. Jérôme, A.-S. Duwez and C. Detrembleur, *Journal of Materials Chemistry*, 2011, 21, 7901-7904.

25. N. Aouina, F. Balbaud-Célérier, F. Huet, S. Joiret, H. Perrot, F. Rouillard and V. Vivier, *Electrochim. Acta*, 2011, 56, 8589-8596.

26. N. Aouina, F. Balbaud-Célérier, F. Huet, S. Joiret, H. Perrot, F. Rouillard and V. Vivier, *Electrochim. Acta*, 2013, 104, 274-281.

27. A. Shahryari and S. Omanovic, *Electrochem. Commun.*, 2007, 9, 76-82.

28. T. Hanawa, *Mat. Sci. Eng. C*, 2004, 24, 745-752.

29. M. Capitan, S. Lefebvre, A. Traverse, A. Paul and J. Odriozola, *Journal of Materials Chemistry*, 1998, 8, 2293-2298.

30. J. Amalric, P. H. Mutin, G. Guerrero, A. Ponche, A. Sotto and J.-P. Lavigne, *Journal of Materials Chemistry*, 2009, 19, 141-149.

31. D. A. López, N. C. Rosero-Navarro, J. Ballarre, A. Durán, M. Aparicio and S.

Ceré, *Surf. Coat. Tech.*, 2008, 202, 2194-2201.

32. A. Sharifnabi, M. Fathi, B. Eftekhari Yekta and M. Hossainalipour, *Appl. Surf. Sci.*, 2014, 288, 331-340.

33. L. Ćurković, H. O. Ćurković, S. Salopek, M. M. Renjo and S. Šegota, *Corros. Sci.*, 2013, 77, 176-184.

34. Y. Zhu, L. Zhang, L. Wang, Y. Fu and L. Cao, *Journal of Materials Chemistry*, 2001, 11, 1864-1868.

35. L. Aries, L. Alberich, J. Roy and J. Sotoul, *Electrochim. Acta*, 1996, 41, 2799-2803.

36. P. Ming, W. Lv, Y. Li, J. Shang and J. Wang, *Electrochim. Acta*, 2014, 120, 6-15.

37. D. Nickolova, E. Stoyanova, D. Stoychev, I. Avramova and P. Stefanov, *Surf. Coat. Tech.*, 2008, 202, 1876-1888.

38. A. Oskuie, A. Afshar and H. Hasannejad, *Surf. Coat. Tech.*, 2010, 205, 2302-2306.

39. N. Ö. Pekmez, K. Cınkıllı and B. Zeybek, *Prog. Org. Coat.*, 2014, 77, 1277-1287.

40. H. Wang, G. Teeter and J. A. Turner, *Journal of Materials Chemistry*, 2011, 21, 2064-2066.

41. K. Nikolov, K. Köster, P. Kaestner, G. Bräuer and C.-P. Klages, *Vacuum*, 2014, 102, 31-37.

42. K. Köster, P. Kaestner, G. Bräuer, H. Hoche, T. Troßmann and M. Oechsner,

Surf. Coat. Tech., 2013, 228, S615-S618.

43. J. Buhagiar, A. Spiteri, M. Sacco, E. Sinagra and H. Dong, *Corros. Sci.*, 2012, 59, 169-178.

44. C. Li and T. Bell, *Corros. Sci.*, 2006, 48, 2036-2049.

45. W. Rausch, *The phosphating of metals*, 1990.

46. T. Sankara Narayanan, S. Jegannathan and K. Ravichandran, *Prog. Org. Coat.*, 2006, 55, 355-362.

47. Y.-M. Kuo, *Journal of hazardous materials*, 2012, 201, 265-272.

48. N. Rezaee, M. Attar and B. Ramezanzadeh, *Surf. Coat. Tech.*, 2013, 236, 361-367.

49. S. Jegannathan, T. Sankara Narayanan, K. Ravichandran and S. Rajeswari, *Surf. Coat. Tech.*, 2006, 200, 4117-4126.

50. A. J. Bard, *Encyclopedia of Electrochemistry: Corrosion and oxide films*, Wiley-VCH Verlag GmbH: Weinheim, Germany, 2003, 2003.

51. E. I. Ghali and R. Potvin, *Corros. Sci.*, 1972, 12, 583-594.

52. R. A. Gittens, T. McLachlan, R. Olivares-Navarrete, Y. Cai, S. Berner, R. Tannenbaum, Z. Schwartz, K. H. Sandhage and B. D. Boyan, *Biomaterials*, 2011, 32, 3395-3403.

53. T. Osathanon, K. Bespinyowong, M. Arksornnukit, H. Takahashi and P. Pavasant, *J. Oral Sci.*, 2011, 53, 23-30.

54. A. Valanezhad, K. Tsuru, M. Maruta, G. Kawachi, S. Matsuya and K. Ishikawa, *Surf. Coat. Tech.*, 2012, 206, 2207-2212.

55. C. Andrade and C. Alonso, *Mater. Struct.*, 2004, 37, 623-643.

56. V. de Freitas Cunha Lins, G. F. de Andrade Reis, C. R. de Araujo and T. Matencio, *Appl. Surf. Sci.*, 2006, 253, 2875-2884.

57. J. Creus, H. Mazille and H. Idrissi, *Surf. Coat. Tech.*, 2000, 130, 224-232.

58. X. Zhang, Z. H. Jiang, Z. P. Yao, Y. Song and Z. D. Wu, *Corros. Sci.*, 2009, 51, 581-587.

59. Y. Wang, Y. Zheng, S. Wei and M. Li, *J. Biomed. Mater. Res. B*, 2011, 96, 34-46.

60. E. Banczek, P. Rodrigues and I. Costa, *Surf. Coat. Tech.*, 2006, 201, 3701-3708.

61. M. Mahdavian and M. Attar, *Corros. Sci.*, 2006, 48, 4152-4157.

62. G. Goeminne, H. Terryn and J. Vereecken, *Electrochim. Acta*, 1998, 43, 1829-1838.

63. Y. Guo, W. Li, L. Zhu and H. Liu, *Mater. Lett.*, 2012, 72, 125-127.

64. D. Stanssens, H. Van den Abbeele, L. Vonck, G. Schoukens, M. Deconinck and P. Samyn, *Mater. Lett.*, 2011, 65, 1781-1784.

65. Y. Z. Guo, W. P. Li, L. Q. Zhu, Z. W. Wang and H. C. Liu, *Appl. Surf. Sci.*, 2012, 259, 356-361.

66. A. Uyama, S. Yamazoe, S. Shigematsu, M. Morimoto, S. Yokojima, H. Mayama, Y. Kojima, S. Nakamura and K. Uchida, *Langmuir*, 2011, 27, 6395-6400.

67. M. Sato, E. B. Slamovich and T. J. Webster, *Biomaterials*, 2005, 26,

1349-1357.